# Capillary effects during droplet impact on a solid surface

M. Pasandideh-Fard, Y. M. Qiao, S. Chandra, and J. Mostaghimi
*Department of Mechanical Engineering, University of Toronto, Toronto, Ontario, M5S 1A4 Canada*

(Received 28 June 1995; accepted 13 November 1995)

Impact of water droplets on a flat, solid surface was studied using both experiments and numerical simulation. Liquid–solid contact angle was varied in experiments by adding traces of a surfactant to water. Impacting droplets were photographed and liquid–solid contact diameters and contact angles were measured from photographs. A numerical solution of the Navier–Stokes equation using a modified SOLA-VOF method was used to model droplet deformation. Measured values of dynamic contact angles were used as a boundary condition for the numerical model. Impacting droplets spread on the surface until liquid surface tension and viscosity overcame inertial forces, after which they recoiled off the surface. Adding a surfactant did not affect droplet shape during the initial stages of impact, but did increase maximum spread diameter and reduce recoil height. Comparison of computer generated images of impacting droplets with photographs showed that the numerical model modeled droplet shape evolution correctly. Accurate predictions were obtained for droplet contact diameter during spreading and at equilibrium. The model overpredicted droplet contact diameters during recoil. Assuming that dynamic surface tension of surfactant solutions is constant, equaling that of pure water, gave predicted droplet shapes that best agreed with experimental observations. When the contact angle was assumed constant in the model, equal to the measured equilibrium value, predictions were less accurate. A simple analytical model was developed to predict maximum droplet diameter after impact. Model predictions agreed well with experimental measurements reported in the literature. Capillary effects were shown to be negligible during droplet impact when $We \gg Re^{1/2}$.  [S1070-6631(96)01203-2]

## I. INTRODUCTION

Modeling industrial processes such as spray cooling of hot surfaces, fire extinguishment by sprinkler systems, plasma coating, spray forming, and pesticide spraying requires an understanding of the impact dynamics of liquid drops on solid surfaces. Several simple analytical models of droplet impact have been proposed,[1–5] based on an energy balance that equates initial droplet kinetic energy to change in surface energy due to droplet deformation and work done in overcoming liquid viscosity during impact. Bennett and Poulikakos[6] have reviewed the use of such models in predicting the maximum diameter of droplet spread, after which further spreading is restrained by liquid surface tension and viscosity. These models, however, give no information about pressure, velocity, and temperature distributions during droplet deformation. Calculations of heat transfer between a surface and impinging droplets require detailed information about droplet shape and temperature during impact, which can be obtained only by a complete solution of the continuity, momentum, and energy equations.

Harlow and Shannon[7] were the first to obtain a numerical solution to the problem of fluid flow during droplet impact, using the so-called ''Marker-and-Cell'' (MAC) finite difference method to solve the Navier–Stokes equations. They neglected any effects of liquid surface tension and viscosity, so that their results are applicable only to the initial stages of droplet impact when these forces are negligible compared to inertial effects. Their solution could not predict the maximum extent of liquid spread, but proved useful in research on erosion of turbine blades by high-speed impinging droplets to calculate peak liquid pressures immediately after impact.[8,9] Modeling heat transfer within the droplet required modifications to the MAC code to include surface tension and viscous effects, which was done by Tsurutani *et al.*[10] and Watanabe *et al.*[11] An alternate algorithm for solving the complete Navier–Stokes equations, the ''Volume-of-Fluid'' (VOF) method, was used by Liu *et al.*[12] and Pasandideh-Fard and Mostaghimi[13] to model spreading and simultaneous solidification of molten droplets on a substrate during plasma spraying. A commercially available code (FLOW-3D) that implements the VOF method to model three-dimensional, unsteady, free surface flows, was used by Trapaga *et al.*[14,15] to study fluid flow, heat transfer and solidification during molten metal droplet impact. Fukai *et al.*[16] studied the fluid dynamics of droplet impact using a finite element method and a varying, rather than fixed, discretization grid to improve solution accuracy when the droplet underwent large deformations.

An accurate description of fluid flow at the liquid–solid–gas contact line is important in formulating realistic models of droplet impact. Analytical solutions have been derived[17,18] to predict fluid flow during capillarity-driven spreading of droplets deposited gently on a solid surface. Modeling fluid behavior in the vicinity of a moving contact line is complicated, because assuming a no-slip boundary

condition at the solid–liquid interface leads to a force singularity at the contact line.[17] The problem can be resolved by replacing the no-slip boundary condition with a slip model.[19] Though this method alleviates mathematical difficulties, there is no experimental evidence to determine which of several available slip models is the most appropriate one to use, or whether slip does indeed occur.

Fluid motion in droplets impinging with significant velocity on a surface is controlled by inertial in addition to capillary forces, and no analytical solution is available for the flow problem. Numerical models of droplet impact usually specify the contact line boundary condition by assigning a value to the angle between the solid surface and the liquid–gas interface. This apparent contact angle defines the shape of the free liquid surface above the contact line. Though the contact angle can, in principle, be measured directly, no experimental measurements of contact angle variation during droplet impact and spread are available in the literature. Trapaga *et al.*[14,15] and Pasandideh-Fard and Mostaghimi[13] therefore assumed contact angles remain constant, with arbitrarily selected values ranging from 5° to 90°. Rather than assuming an arbitrary contact angle, Fukai *et al.*[16] neglected capillary forces at the contact line. They noted, however, that capillary forces become increasingly important toward the end of droplet spreading when inertial forces become small, and that model results would be sensitive to capillary effects at this time. In a subsequent paper,[20] they used experimentally determined values of advancing and receding contact angles, measured from photographs of droplets sliding down an inclined surface, and found that model predictions improved.

A study of surface wetting effects during droplet impact is important, not only in accurately modeling industrial applications of liquid sprays, but also in improving them. In particular, wetting of solid surfaces by droplets can be enhanced by dissolving a surfactant in the liquid to reduce the contact angle. Addition of surfactant solutions, known as ''wetting agents,'' to water sprays, is known to reduce the amount of water required to extinguish fires.[21] The use of surfactants has also been proposed to improve coverage of foliage by liquid pesticide sprays.[1] In spite of these practical applications, no study is available in the literature that describes the effect of dissolved surfactant on impact dynamics of droplets.

We studied, using both experiments and numerical modeling, the effect of adding a surfactant to water drops impacting a stainless steel surface. Our objectives were to (a) observe experimental changes in droplet impact dynamics produced by dissolved surfactant; (b) measure liquid–solid contact angle during droplet impact; (c) verify that the numerical model accurately predicted droplet shape during deformation, using measured contact angle values; (d) study the effect of using a constant, rather than dynamic, contact angle in formulating the model; (e) determine the effect of a surfactant on dynamic surface tension values; and (f) develop a simple criteria to determine conditions under which capillary effects can be neglected when modeling droplet impact.

Surfactant concentration in water was the principal parameter varied—from 0 to 1000 ppm by weight—in our experiments. Droplet diameter ($2.05\pm0.03$ mm) and impact velocity (1.0 m/s) were held constant. Photographs were taken of droplets impacting on a stainless steel surface, from which we measured variation of the liquid–solid contact angle and contact diameter during droplet spreading. We used the numerical model of Pasandideh-Fard and Mostaghimi[13] to calculate the evolution of droplet shapes during impact, using both equilibrium contact angles and measured values of dynamic contact angles, and compared predicted values with experimental measurements.

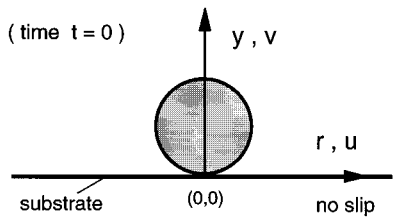


FIG. 1. Initial configuration used in numerical computations.

## II. NUMERICAL METHOD

Figure 1 shows the axisymmetric coordinate system used in formulating the numerical model, and the initial configuration of the droplet at the time of impact, $t=0$. The mathematical model assumed that droplet impingement velocity was normal to the substrate, and that fluid flow was laminar and incompressible. Due to the large deformation undergone by an impacting droplet, an Eulerian formulation was used. The governing equations may be written, using axisymmetric coordinates, as follows: *Continuity equation*:

$$\frac{\partial u}{\partial r}+\frac{\partial \nu}{\partial y}+\frac{u}{r}=0,\neg \tag{1}$$

where $u$ and $\nu$ are velocity components in the $r$ and $y$ directions, respectively (Fig. 1); *momentum equations*:

$$\frac{\partial u}{\partial t}+u\frac{\partial u}{\partial r}+\nu\frac{\partial u}{\partial y}$$
$$=\frac{-1}{\rho}\frac{\partial P}{\partial r}+\nu\left(\frac{\partial^2 u}{\partial r^2}+\frac{\partial^2 u}{\partial y^2}+\frac{1}{r}\frac{\partial u}{\partial r}-\frac{u}{r^2}\right)+g_r,\neg \tag{2}$$

$$\frac{\partial \nu}{\partial t}+u\frac{\partial \nu}{\partial r}+\nu\frac{\partial \nu}{\partial y}=\frac{-1}{\rho}\frac{\partial P}{\partial y}+\nu\left(\frac{\partial^2 \nu}{\partial r^2}+\frac{\partial^2 \nu}{\partial y^2}+\frac{1}{r}\frac{\partial \nu}{\partial r}\right)+g_y, \tag{3}$$

where $P$, $\rho$, and $\nu$ are pressure, density, and kinematic viscosity of the fluid, respectively, and $g$ represents gravitational force per unit mass.

To represent the free boundaries of the droplet, the ''fractional volume of fluid'' scheme was used. In this technique, a function $F(r,y,t)$ was defined whose value was equal to the fractional volume of the cell occupied by the fluid. Here $F$ equaled one for cells occupied by the fluid and zero for empty cells. Cells with values of $0<F<1$ contained a free surface. Since $F$ moved with the fluid (i.e., the total value of $F$ for the droplet was constant) this function satisfied the conservation equation:

$$\frac{DF}{Dt} = \frac{\partial F}{\partial t} + u\frac{\partial F}{\partial r} + \nu\frac{\partial F}{\partial y} = 0.\neg \tag{4}$$

Boundary conditions for the flow problem are shown in Fig. 1. The flow was assumed symmetrical about the $y$ axis, with no slip at the solid substrate. At a free surface tangential stresses were set equal to zero and normal stresses were replaced by an equivalent surface pressure, calculated from the interface mechanical equilibrium condition given by the Laplace equation:

$$P_1 - P_v = J\gamma, \tag{5}$$

where $P_1$ and $P_v$ were pressures inside and outside the droplet, respectively, $J$ was the interface mean curvature, and $\gamma$ was the liquid–gas surface tension.

Describing the liquid–solid contact line required special attention. We incorporated the contact angle, $\theta$, in the free surface boundary condition [Eq. (5)] by using it to calculate the mean curvature, $J$, of the liquid meniscus near the substrate. The technique has earlier been described in detail by Nichols, Hirt, and Hotchkiss.[22] The model used either a constant value of $\theta$, or a dynamic contact angle that varied with time during droplet impact. When dynamic contact angle values were used, they were updated after each time step.

The equations were solved using the modified SOLA-VOF numerical code, a program based on the ''Marker and Cell'' finite-difference technique. Most terms in the momentum equations were solved using an explicit computational scheme, but the coupling between pressures and velocities was implicit. This semi-implicit formulation was solved using the successive over-relaxation method to accelerate convergence.

## III. EXPERIMENTAL METHOD

Single droplets were formed by forcing water from a syringe pump through a hypodermic needle and letting them detach under their own weight. Droplets fell onto a polished stainless steel surface placed 50 mm below the needle tip. Their impact velocity, 1 m/s, was low enough that droplets did not shatter upon impact. Photographs of droplet impact were taken using a single-shot flash photographic technique (described in detail by Chandra and Avedisian[3]). A strobe unit with an 8 $\mu$s flash duration provide illumination to take a single 35 mm photograph of a droplet at one instant during its impact. By varying the time delay between the droplet first touching the surface and triggering of the flash, different stages of droplet impact could be photographed. Droplet release and impact were sufficiently repeatable that the entire droplet deformation process could be reconstructed from photographs of different droplets, captured at progressively advancing stages of impact.

The surfactant used in experiments was sodium dodecyl sulphate (SDS), obtained in the form of a powder from Malinckrodt Speciality Chemicals. Three different surfactant concentrations were used in experiments: 0 (i.e., pure water), 100, and 1000 ppm by weight. These concentrations were low enough that changes in density and viscosity were negligible. We determined the variation of surface tension with surfactant concentration by measuring diameters of spherical droplets photographed in freefall, after they had detached from the needle tip. Surface tension values were calculated by equating the weight of each droplet to the surface tension force attaching it to the needle tip, whose diameter was known. This method was tested using pure water and $n$-heptane: measured surface tensions agreed closely with values reported in the literature. Adding increasing amounts of the surfactant reduced the measured surface tension from 73 (pure water) to 70 (100 ppm), and 50 mN/m (1000 ppm), respectively. A 33 gauge hypodermic needle was used to form droplets of pure water and 100 ppm solutions, and 30 gauge for 1000 ppm solution, which had significantly lower surface tension. Uniform-sized droplets were formed by this method, with diameters of $2.05 \pm 0.03$ mm.

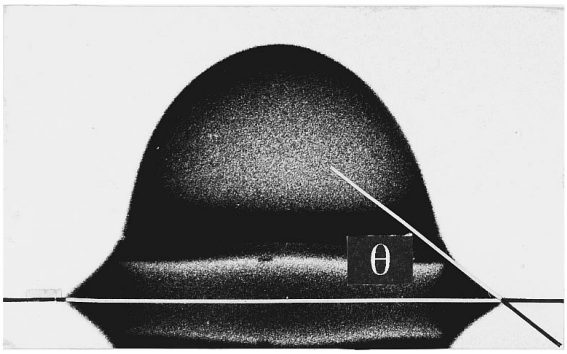


FIG. 2. Liquid–solid contact angle ($\theta$) measurement from a photograph of a droplet of pure water 8.2 ms after impacting a stainless steel surface.

Liquid–solid contact angles and contact diameters (i.e., the diameter of the wetted surface area) were measured from enlarged photographs of droplet impact and spreading by manually drawing a tangent through the liquid–gas interface. Figure 2 shows an example of contact angle measurement from a photograph of a droplet of pure water 8.2 ms after impact. We verified the repeatability of our measurements by photographing five different droplets at the same instant after impact. This was repeated for ten different time delays. Measurements of the contact angle were reproducible within $\pm 2°$, and of contact diameter within $\pm 0.1$ mm.

## IV. RESULTS AND DISCUSSION

Figure 3 shows images of droplet deformation obtained from the numerical model, along with photographs of 2.0 mm diam droplets of pure water impacting the surface with a velocity of 1 m/s. Both computer generated images and photographs are viewed from the same angle (30° from the horizontal), and at the same time ($t$) after impact. Droplets can be seen reflected in the polished stainless steel surface in the photographs. A single bubble formed in droplets at their point of impact because of entrapment of air in a cusp at the liquid–solid interface.[3] No bubbles were seen in theoretically predicted droplet shapes, since the model did not consider pressure changes in the air surrounding droplets. Droplets did not break up during impact since their kinetic energy was too low to overcome surface tension. A measure of the relative magnitudes of kinetic and surface energies is the Weber number ($\mathrm{We} = \rho D_0 V_0^2/\gamma$), whose value was 27 for the condi-

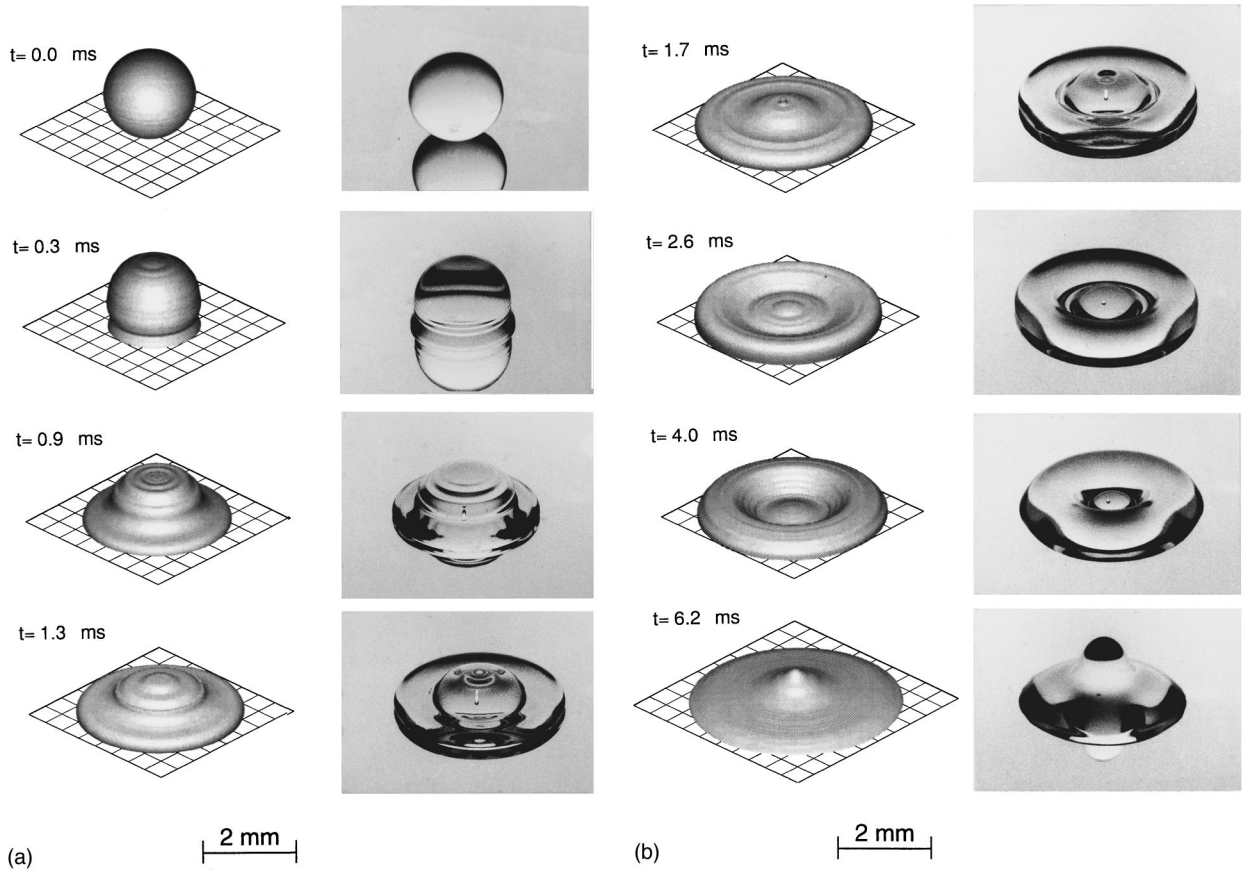


FIG. 3. Computer generated images compared with photographs of a 2 mm diam water droplet impacting a stainless steel surface with a velocity of 1 m/s. The time of each frame ($t$) is measured from impact.

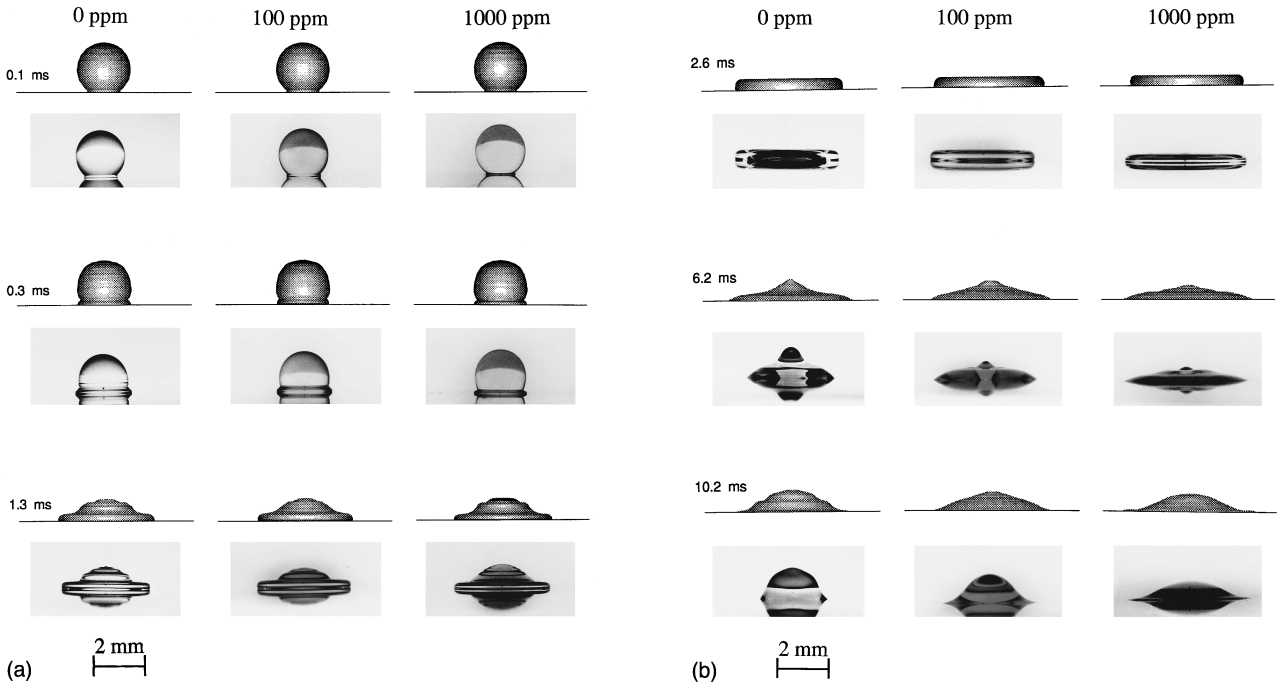


FIG. 4. Comparison of photographs with model predictions for impact of droplets of pure water (0 ppm), 100, and 1000 ppm surfactant solution.

tions of Fig. 3. The droplet reached its maximum extent at approximately $t=2.6$ ms, after which surface tension and viscous forces overcame inertia, so that fluid accumulated at the leading edge of the splat and it started pulling back. Surface tension finally caused recoil of droplets off the surface ($t=6.2$ ms).

The effect of adding a surfactant on droplet impact dynamics can be seen in Fig. 4. Computer simulated images of impacting droplets are compared with photographs taken at the same instant after impact for droplets of pure water (0 ppm), and also for droplets to which 100 and 1000 ppm of surfactant was added. The surfactant appeared to have little influence on early stages of droplet spread: droplet shapes appear similar in all three cases for $t \leqslant 1.3$ ms. The maximum extent of spread increased as more surfactant was added (see Fig. 4, $t=2.6$ ms). Droplet shape during recoil was sensitive to surfactant concentration. Adding as little as 100 ppm of surfactant to water produced significant changes in droplet shape (see Fig. 4, $t=6.2$ ms). A simple order of magnitude analysis[3] shows that during the initial period of droplet spreading inertial forces are much larger than surface tension and viscous forces; lowering surface tension or contact angle therefore has little influence on fluid flow. Droplet recoil, though, is controlled by capillary forces, and adding a surfactant decreases the height of droplet recoil (see Fig. 4, $t=10.2$ ms).

Modeling the effect of a surfactant on the surface tension of a freshly created surface is a complex problem. The surfactant reduces surface tension when it diffuses to the free liquid surface: dynamic surface tension values therefore depend on the age and history of a surface.[23] The surfactant was uniformly distributed in droplets when they formed at the needle tip. Diffusion of SDS in water is relatively slow, with an estimated[24] diffusion coefficient $\alpha=8\times10^{-10}$ m$^2$/s. An order-of-magnitude estimate of the characteristic time for transport of SDS in a droplet by diffusion is $D^2/\alpha$, equaling $5\times10^3$ s for $D=2$ mm. Consequently, a further reduction in surface tension due to the migration of surfactant to the free surface, would be negligible in the $10^{-2}$ s period of droplet impact. Therefore, our measurement of surface tension, made at the instant the droplet detached, represented a lower bound on possible surface tension values. However, as the droplet deformed during impact, the depletion of surfactant due to the expansion of free surface area may have increased surface tension. Experiments[25] on the rapid growth of bubbles in aqueous surfactant solutions have shown that dynamic surface tension can equal that of pure liquid. Surface tension values during the impact of surfactant solution droplets could, therefore, lie between that of pure water (73 mN/m) and those measured by us experimentally (70 mN/m for 100 ppm and 50 mN/m for 1000 ppm surfactant), and also vary from point to point on the droplet surface.

We did not attempt to model the transport of surfactant during droplet impact. Any assumptions made in such a model would have been unverifiable because we had no means of experimentally measuring surface tension distributions during droplet deformation. Instead we calculated droplet shapes during impact using the highest and lowest values of surface tension (that of pure water, and our experimentally measured value) to determine if changes in surface tension significantly altered the results. The two sets of results were compared with experimental measurements to see which gave better agreement. A quantitative comparison of experimental and numerical results was done by measuring the diameter of the wetted surface area ($D$) at successive stages during droplet deformation. Normalizing this quantity by the initial droplet diameter ($D_0$) yields the so-called "spread factor," $\xi(t)=D(t)/D_0$. Experimentally measured values of $\xi$ are shown by the symbols in Fig. 5 for droplets containing 1000 ppm of surfactant; solid lines mark model predictions obtained using two different values of $\gamma$. Results are shown for both small times after impact ($t^*<3.5$, where $t^*=tV_0/D_0$) to show details of impact, and large times ($5<t^*<30$) to show equilibrium. Results obtained from the two calculations showed little difference. Assuming any surface tension value in the range 50 mN/m$\leqslant\gamma\leqslant$73 mN/m would have produced reasonable predictions for the evolution of $\xi$. Similar calculations for 100 ppm surfactant solution droplets, using surface tension values of 70 and 73 mN/m, revealed only very minor differences between values of $\xi$. However, Fig. 5 shows that using $\gamma=73$ mN/m gave better predictions for $\xi$ during the period $3<t^*<10$. Qualitative inspection of predicted droplet shapes showed that they were sensitive to surface tension values during this time, when the droplet was recoiling. Figure 6 shows images of impacting 1000 ppm droplets at $t=6.2$ and 10.2 ms, calculated using the two different values of $\gamma$. Comparison with photographs (Fig. 4) confirms that using $\gamma=73$ mN/m gave predictions that were in close agreement with experimental

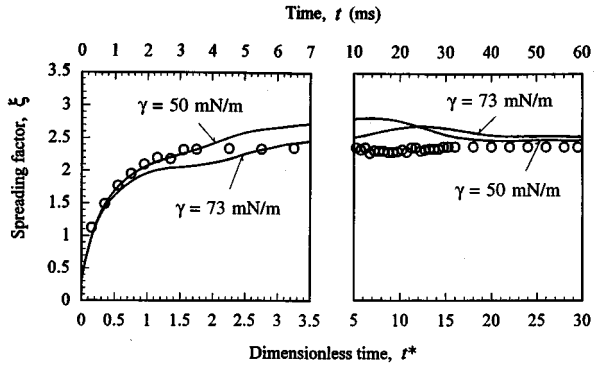


FIG. 5. Variation of measured spread factor ($\xi$), shown by symbols, during impact of a droplet with 1000 ppm of surfactant, compared with model predictions (solid lines) using surface tension ($\gamma$) values of 50 and 73 mN/m.

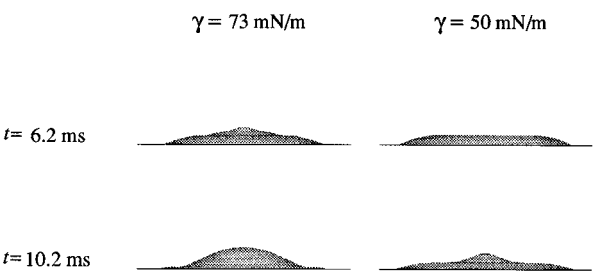


FIG. 6. Shapes of impacting 1000 ppm surfactant solution droplets calculated using surface tension ($\gamma$) values of 50 and 73 mN/m.

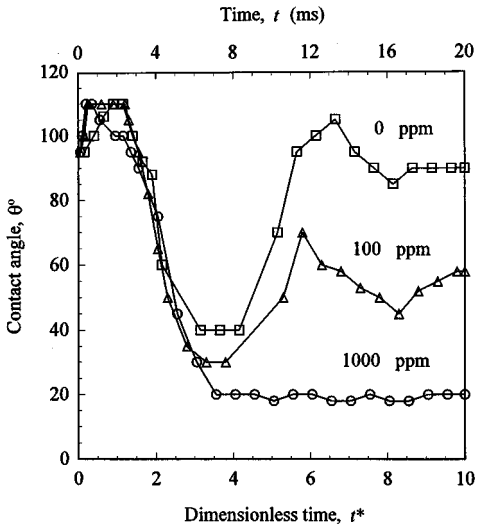


FIG. 7. Measured evolution of the contact angle during spreading of droplets of pure water (0 ppm), 100, and 1000 ppm surfactant solution.

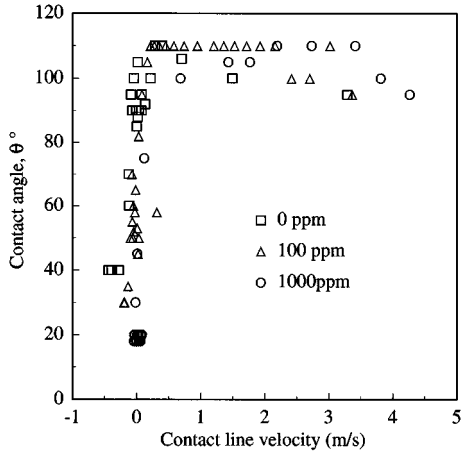


FIG. 8. Variation of the contact angle with contact line velocity.

observations, suggesting that dynamic surface tension values of surfactant solutions were, indeed, close to that of pure water. All calculations in this paper were performed, therefore, assuming surface tension equal to 73 mN/m.

Since surface tension was assumed constant in the model, adding a surfactant affected impact dynamics, only because it reduced the liquid–solid contact angle. Model results shown in Figs. 3 and 4 were obtained using experimentally measured dynamic contact angle values. Figure 7 shows measured values of contact angles ($\theta$) during droplet impact and rebound. Symbols in Fig. 7 mark experimental measurements; linear interpolation was used in calculations to estimate intermediate values. In all three cases (0, 100, and 1000 ppm), the advancing contact angle ($\theta_a$), measured during droplet spreading ($t^*<1.5$), remained approximately constant ($\sim$110°), regardless of surfactant concentration. Once droplets reached their maximum extension surface tension forces caused recoil ($1.5<t^*<3$). Splat diameters remained constant while contact angles decreased until they reached their minimum value, called the receding contact angle, at $t^*\approx 3$. The periphery of the splat was then drawn inward, reaching its final position at $t^*\approx 4$. Droplets assumed their equilibrium forms, shaped like spherical caps, at $t^*>10$. Measured equilibrium contact angle values were: pure water, 90°; 100 ppm surfactant solution, 57°; and 1000 ppm surfactant solution, 18°.

Dynamic contact angles are known to increase with the velocity of a moving solid–liquid–air contact line.[26,27] Elliot and Riddiford[26] measured contact angles during liquid flow between two parallel plates, and found that advancing contact angles increased linearly with contact line velocity, until finally an upper limiting value of $\theta_a$ was reached: contact angles were then independent of further increases in velocity. They also determined that the addition of a surfactant did not change this maximum value of $\theta_a$. Contact line velocities in our experiments were estimated by differentiating polynomial curves fitted through measurements of droplet contact diameter evolution. Figure 8 shows the variation of dynamic contact angles with contact line velocity; positive velocities indicate droplet spreading and negative velocities recoil. Our measurements confirm that values of advancing contact angles reach a maximum of approximately 110°, independent of both contact line velocity and surfactant concentration.

We performed calculation using a constant, as done in previous studies,[13–16] rather than a dynamic contact angle to see if this increased errors in model predictions. Measured values for $\xi$ for droplets of pure water are indicated in Fig. 9(a) by symbols. Numerical predictions are shown by solid lines for simulations done using both measured values of dynamic contact angle, and constant contact angle set equal to the equilibrium value. For pure water the equilibrium contact angle (90°) was close to the advancing contact angle ($\sim$100°; see Fig. 7). Consequently, there was little difference between the results of the two simulations, and both accurately predicted experimental measurements during droplet spreading [Fig. 9(a), $t^*<2$]. However, during droplet recoil ($2.5<t^*<10$) there was a considerable discrepancy between numerical predictions and measured values of $\xi$. As the droplet recedes it leaves a very thin liquid film behind on the surface (Fig. 4, $t=10.2$ ms). Modeling fluid flow realistically in this thin layer presents considerable challenges. It is not clear whether it is appropriate to use a no-slip boundary condition in this situation, or whether our measured values of $\theta_a$ differ from actual contact angles near the surface. When the droplet reached an equilibrium shape predicted values once again agreed well with measurements [Fig. 9(a), $t^*>15$].

A comparison between measured and predicted values of $\xi$ for droplets containing 100 ppm surfactant is shown in Fig. 9(b). In this case the equilibrium contact angle (57°) was much lower than the advancing contact angle ($\sim$110°, see Fig. 7). Results from the model assuming a constant contact angle, therefore, overestimated $\xi$ during droplet spreading. Using dynamic contact angle values gave much more accurate results, but both models predicted larger values of contact diameter than seen in experiments. Similar measurements and calculations for droplets with 1000 ppm surfactant are seen in Fig. 9(c). The dynamic contact angle model predicted droplet diameter evolution reasonably accurately during the entire impact process. Assuming a constant contact

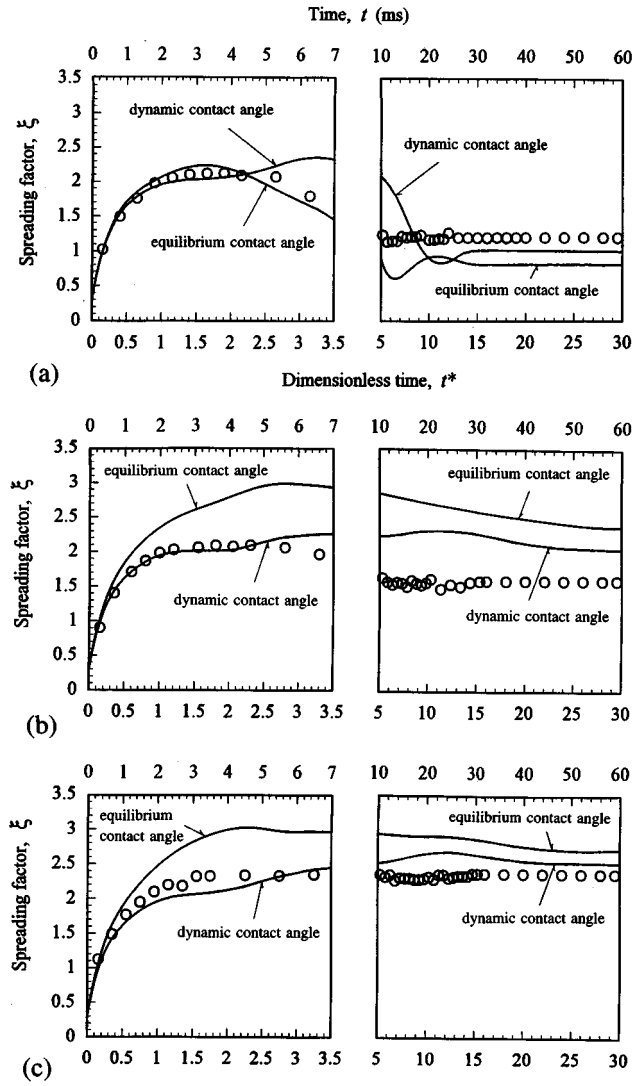


FIG. 9. Evolution of calculated (lines) and measured (symbols) spread factors during impact of (a) pure water droplet, (b) 100 ppm surfactant solution, and (c) 1000 ppm surfactant solution.

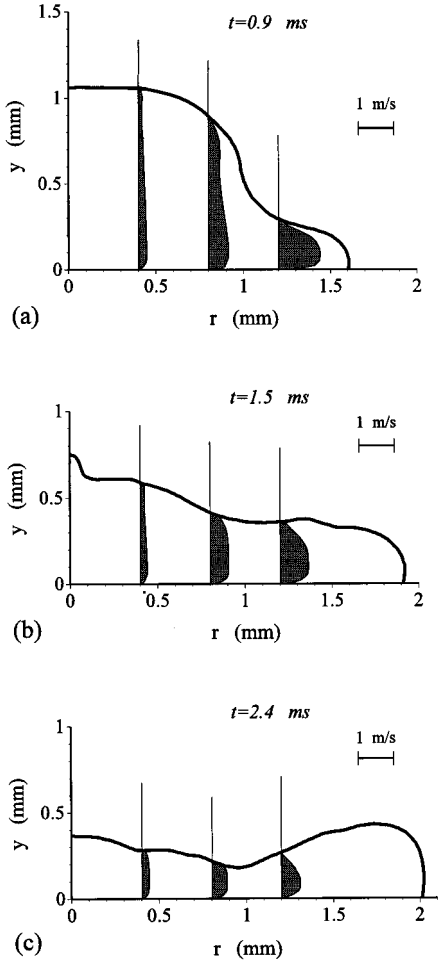


FIG. 10. Predicted droplet shape and velocity distribution at (a) $t=0.9$ ms, (b) $t=1.5$ ms, and (c) $t=2.4$ ms.

angle, however, made the model overpredict $\xi$ by up to 30%.

Using values of equilibrium, rather than dynamic, contact angle was found to produce significant errors when modeling droplet impact in our experiments, where impact velocity was low (1 m/s). However, as impact velocity increases droplet kinetic energy will become much larger than surface energy (i.e., Weber number will become large), and surface tension and contact angle effects will eventually become negligible. A criteria to establish conditions under which capillary effects are negligible can be obtained from a simple energy conservation model of droplet spread. Several such models are available in the literature and have been reviewed in detail by Bennett and Poulikakos.[6] The equation derived here is an extension of that developed by Chandra and Avedisian.[3]

Before impact, the kinetic energy ($KE_1$) and surface energy ($SE_1$) of a spherical droplet are given by

$$\mathrm{KE}_1=\left(\frac{1}{2}\rho V_0^2\right)\left(\frac{\pi}{6}D_0^3\right),\neg \tag{6}$$

$$\mathrm{SE}_1=\pi D_0^2\gamma.\neg \tag{7}$$

After impact, when the droplet is at its maximum extension diameter $D_{\max}$, the kinetic energy is zero and the surface energy ($SE_2$) is[28]

$$\mathrm{SE}_2=\frac{\pi}{4}D_{\max}^2\gamma(1-\cos\,\theta_a).\neg \tag{8}$$

The work done in deforming the droplet against viscosity is approximately[3]

$$W=\int_0^{t_c}\int_\Omega \phi\; d\Omega\; dt\approx\phi\Omega t_c,\neg \tag{9}$$

where $\Omega$ is the volume of viscous fluid, $t_c$ is the time taken for the droplet to spread, and $\phi$ is the viscous dissipation function. The magnitude of $\phi$ is estimated by[3]

$$\phi\sim\mu\left(\frac{V_0}{L}\right)^2,\neg \tag{10}$$

where $\mu$ is the liquid viscosity and $L$ is a characteristic length in the $y$ direction. Chandra and Avedisian[3] assumed $L$ equals the splat thickness $h$. Their results overestimated $D_{\max}$ values by up to 40%, suggesting that $L$ is, in fact, smaller than $h$. Therefore, a more appropriate length scale to esti-

mate the magnitude of viscous dissipation may be the boundary layer thickness ($\delta$) at the solid–liquid interface. Figures 10(a)–10(c) shows calculated droplet shapes and velocity profiles at three different locations in an impacting water drop, at three different instants during droplet spread. Thecalculated value of $\delta$ is approximately 0.1 mm, and does not change significantly with position or time while the droplet is spreading.

We obtained an analytical expression for the boundary layer thickness by assuming that liquid motion in the droplet can be represented by axisymmetric stagnation point flow. The streamfunction ($\psi$) for potential flow outside the boundary layer in such a flow is[29]

$$\psi = -Br^2 y, \tag{11}$$

where $B$ is a constant. The liquid velocity component normal to the wall $V_y = -2By$; assuming $V_y = -V_0$ at $y = D_0/2$ gives $B = V_0/D_0$. With the free-stream velocity distribution described by the streamfunction of Eq. (11), a similarity solution for boundary layer flow can be obtained.[29] The boundary layer thickness is given by

$$\delta = 2\frac{D_0}{\sqrt{\mathrm{Re}}}, \tag{12}$$

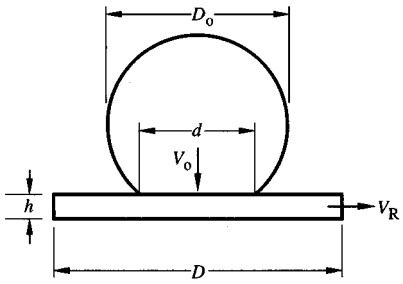


FIG. 11. Model of droplet spreading.

where the Reynolds number $\mathrm{Re} = V_0 D_0/\upsilon$. Substituting values of $\upsilon$, $D_0$, and $V_0$ from our experiments in Eq. (12) gives $\delta = 0.09$ mm, in good agreement with predictions from the numerical model [see Figs. 10(a)–10(c)].

The time ($t_c$) required for a liquid droplet to reach the maximum splat diameter can be estimated by assuming the drop spreads into a cylindrical disk of diameter $D$ and thickness $h$ (Fig. 11). Liquid flows from the drop, shaped like a truncated sphere, into the film through an area of diameter $d$ with velocity $V_0$. The velocity at the edge of the splat during spreading ($V_R$) is given by conservation of mass to be

$$\frac{V_R}{V_0} = \frac{d^2}{4\,Dh}. \tag{13}$$

TABLE I. Comparison of measured values of $\xi_{\max}$ with predictions from Eq. (18).

| Droplet/Surface | $D_0$ (mm) | $V_0$ (m/s) | We | Re | $\theta_a$° | $\xi_{\max}$ measured | $\xi_{\max}$ calculated | Reference |
|---|---|---|---|---|---|---|---|---|
| Water (SDS 0 ppm)/steel | 2.05 | 1.00 | 27 | 2112 | 110 | 2.15 | 2.47 | [b] |
| Water (SDS 100 ppm)/steel | 2.02 | 1.00 | 27 | 2112 | 110 | 2.16 | 2.47 | [b] |
| Water (SDS 1000 ppm)/steel | 2.07 | 1.00 | 28 | 2112 | 110 | 2.62 | 2.49 | [b] |
| Water/beeswax | 0.616 | 2.61 | 59 | 2084 | 111 | 2.65 | 2.77 | 1 |
| Water/beeswax | 0.776 | 3.29 | 118 | 3298 | 111 | 3.18 | 3.25 | 1 |
| Water/beeswax | 0.888 | 3.71 | 171 | 4258 | 111 | 3.45 | 3.55 | 1 |
| Water/beeswax | 0.977 | 4.00 | 219 | 5057 | 111 | 3.79 | 3.75 | 1 |
| Water/beeswax | 1.053 | 4.28 | 271 | 5833 | 111 | 3.91 | 3.94 | 1 |
| Water/cellulose acetate | 0.616 | 2.61 | 59 | 2084 | 62 | 3.15 | 3.24 | 1 |
| Water/cellulose acetate | 0.776 | 3.29 | 118 | 3298 | 62 | 3.56 | 3.64 | 1 |
| Water/cellulose acetate | 0.888 | 3.71 | 171 | 4258 | 62 | 3.82 | 3.89 | 1 |
| Water/cellulose acetate | 0.977 | 4.00 | 219 | 5057 | 62 | 4.10 | 4.08 | 1 |
| Water/cellulose acetate | 1.053 | 4.28 | 271 | 5833 | 62 | 4.24 | 4.23 | 1 |
| Water/glass | 0.616 | 2.61 | 59 | 2084 | 27 | 3.47 | 3.59 | 1 |
| Water/glass | 0.776 | 3.29 | 118 | 3298 | 27 | 4.07 | 3.90 | 1 |
| Water/glass | 0.888 | 3.71 | 171 | 4258 | 27 | 4.20 | 4.12 | 1 |
| Water/glass | 0.977 | 4.00 | 219 | 5057 | 27 | 4.30 | 4.27 | 1 |
| Water/glass | 1.053 | 4.28 | 271 | 5833 | 27 | 4.40 | 4.42 | 1 |
| Heptane/stainless steel | 1.50 | 0.93 | 43 | 2300 | 20 | 4.00 | 3.82 | 3 |
| Paraffin wax/aluminum | 2.99 | 0.50 | 26 | 213 | 140 | 2.20 | 1.75 | 30 |
| Paraffin wax/aluminum | 2.99 | 1.00 | 102 | 427 | 140 | 2.50 | 2.13 | 30 |
| Paraffin wax/aluminum | 2.99 | 1.50 | 230 | 641 | 140 | 2.60 | 2.41 | 30 |
| Paraffin wax/aluminum | 2.99 | 2.00 | 410 | 854 | 140 | 2.70 | 2.62 | 30 |
| Paraffin wax/aluminum | 2.99 | 2.50 | 641 | 1067 | 140 | 3.00 | 2.80 | 30 |
| Tin/$Al_2O_3$ | 2.70 | 3.70 | 447 | 35 339 | 140[a] | 5.43 | 5.56 | 5 |
| Tin/$Al_2O_3$ | 2.40 | 3.70 | 398 | 31 412 | 140[a] | 4.96 | 5.36 | 5 |
| Tin/$Al_2O_3$ | 2.10 | 3.70 | 348 | 27 486 | 140[a] | 4.50 | 5.10 | 5 |
| Tin/stainless steel | 2.40 | 2.43 | 170 | 20 565 | 140[a] | 3.82 | 4.26 | 5 |
| Zinc/stainless steel | 3.70 | 3.13 | 305 | 23 687 | 140[a] | 5.34 | 4.90 | 5 |

[a]Assumed value.
[b]Present work.

The splat thickness ($h$) after impact can be calculated by equating the volume of a spherical droplet with diameter $D_0$ to that of a cylinder with height $h$ and diameter $D_{\max}$, giving

$$h = \frac{2D_0^3}{3D_{\max}^2};\neg \tag{14}$$

$d$ varies between 0 and $D_0$ during droplet impact. Assuming an average value $d \sim D_0/2$ and combining Eqs. (13) and (14), gives

$$\frac{dD}{dt} = 2V_R = \frac{3}{16} V_0 \frac{D_{\max}^2}{D_0} \frac{1}{D}.\neg \tag{15}$$

Integrating Eq. (15) gives an expansion for the evolution of splat diameter ($D$):

$$\frac{D}{D_{\max}} = \sqrt{\frac{3}{8} t^*}.\neg \tag{16}$$

From Eq. (16), the dimensionless time required for the droplet to reach its maximum extent ($D = D_{\max}$) is $t_c^* = \frac{8}{3}$, and is independent of impact velocity. Inspection of Figs. 9(a)–9(c) confirms that this estimate agrees reasonably well with experiments.

The energy lost to viscous dissipation can be estimated by substituting Eqs. (10) and (12) in Eq. (9), assuming that $L = \delta, t_c = (8D_0)/(3V_0)$, and $\Omega = \pi D_{\max}^2 \delta/4$, giving

$$W = \frac{\pi}{3} \rho V_0^2 D_0 D_{\max}^2 \frac{1}{\sqrt{\mathrm{Re}}}.\neg \tag{17}$$

Using the energy conservation condition, $\mathrm{KE}_1 + \mathrm{SE}_1 = \mathrm{SE}_2 + W$, and combining Eqs. (6), (7), (8), and (17), we obtain a simple expression for the maximum spread factor:

$$\xi_{\max} = \frac{D_{\max}}{D} = \sqrt{\frac{\mathrm{We} + 12}{3(1 - \cos\,\theta_a) + 4(\mathrm{We}/\sqrt{\mathrm{Re}})}}.\neg \tag{18}$$

The accuracy of predictions from Eq. (18) was tested by comparison with experimental measurements for a variety of droplet–surface combinations, over a wide range of Weber number ($26 < \mathrm{We} < 641$) and Reynolds number ($213 < \mathrm{Re} < 35\,339$) values. The results are given in Table I. Agreement between predicted and measured values was good, the error being less than 15% in most cases. Discrepancies were largest at low Re, when the assumption of a thin boundary layer was no longer valid.

The magnitude of the term $(1 - \cos\,\theta_a)$ in Eq. (18) can be, at most, 2. If $\mathrm{We}/\sqrt{\mathrm{Re}}$ is large in comparison, the value of the contact angle will have little effect on $\xi_{\max}$. We may therefore neglect capillary effects when modeling droplet impact if

$$\mathrm{We} \gg \sqrt{\mathrm{Re}}.\neg \tag{19}$$

If also $\mathrm{We} \gg 12$, Eq. (18) reduces to

$$\xi_{\max} = 0.5\ \mathrm{Re}^{0.25}.\neg \tag{20}$$

Previous analyses[2,5,6] of droplet impact with $\mathrm{We} \to \infty$ have shown $\xi_{\max}$ to be proportional to $\mathrm{Re}^a$, where $a$ is a constant, with values ranging from 0.167 to 0.2.

## V. CONCLUSIONS

We studied the influence of surface tension and contact angle on the impact dynamics of a water droplet falling onto a flat stainless steel surface, using both experiments and numerical modeling. The principal findings were the following.

Comparison of computer generated images with photographs showed that the numerical analysis accurately predicts droplet shape during deformation.

Adding surfactant did not affect droplet spreading significantly; however, it changed droplet shape during recoil. This phenomenon, observed both in numerical simulations and experiments, was attributed to inertia dominating droplet spread and capillary forces dominating droplet recoil.

Equilibrium contact angles were reduced by surfactant addition. However, measured advancing contact angles did not vary significantly with surfactant concentration.

The surfactant did not appear to reduce dynamic surface tension. Using a constant value of surface tension in the model, equal to that of pure water, gave results that best agreed with experimental observations.

When dynamic contact angle values were used in the numerical model, accurate predictions were obtained for droplet diameter during spreading and at equilibrium. The model overpredicted droplet diameters during recoil.

When the contact angle was assumed constant, equal to the measured equilibrium value, model predictions were less accurate. The discrepancy between results obtained using constant and dynamic contact angles was least for pure water drops, where the equilibrium and advancing contact angle had values close to each other.

A simple analytical expression was developed to estimate the maximum spread of a droplet on a surface. Predictions from this model were shown to be in good agreement with the experimental measurements for a variety of droplet–surface combinations, over a large range of We and Re.

Capillary effects can be neglected during droplet impact if $\mathrm{We} \gg \sqrt{\mathrm{Re}}$.


[1] R. E. Ford and C. G. L. Furmidge, "Impact and spreading of spray drops on foliar surfaces," in *Wetting* (Society of Chemical Industry, London, 1967), pp. 417–432.

[2] J. Madejski, "Solidification of droplets on a cold surface," Int. J. Heat Mass Transfer **19**, 1009 (1976).

[3] S. Chandra and C. T. Avedisian, "On the collision of a droplet with a solid surface," Proc. R. Soc. London A **432**, 13 (1991).

[4] A. Karl, K. Anders, and A. Frohn, "Experimental investigation of droplet deformation during wall collisions by image analysis," ASME Exp. Num. Flow Visualization FED **172**, 135 (1993).

[5] H. Fukanuma and A. Ohmori, "Behavior of molten droplets impinging on flat surfaces," *Proceedings of the 7th National Thermal Spray Conference*, Boston, MA, June 1994, pp. 563–568.

[6] T. Bennett and D. Poulikakos, "Splat-quench solidification: Estimating the maximum spreading of a droplet impacting a solid surface," J. Mat. Sci. **28**, 963 (1993).

[7] F. H. Harlow and J. P. Shannon, "The splash of a liquid drop," J. Appl. Phys. **38**, 3855 (1967).

[8] Y. C. Huang, F. G. Hammitt, and W.-J. Yang, "Hydrodynamic phenomena during high-speed collision between liquid droplet and rigid plane," Transactions of the ASME, Journal of Fluids Engineering, June 1973, pp. 276–294.

[9] P. H. Pidsley, "A numerical investigation of water drop impact," *Proceed-*

*ings of the 6th International Conference on Erosion by Liquid and Solid Impact*, 1983, Sec. 18(1-6).
[10]K. Tsurutani, M. Yao, J. Senda, and H. Fujimoto, ''Numerical analysis of the deformation process of a droplet impinging upon a wall,'' JSME Int. J. Ser. (II) **33**, 555 (1990).
[11]T. Watanabe, I. Kuribayashi, T. Honda, and A. Kanzawa, ''Deformation and solidification of a droplet on a cold substrate,'' Chem. Eng. Sci. **47**, 3059 (1992).
[12]H. Liu, E. J. Lavernia, and R. H. Rangel, ''Numerical simulation of substrate impact and freezing of droplets in plasma spray processes,'' J. Phys. D Appl. Phys. **26**, 1900 (1993).
[13]M. Pasandideh-Fard and J. Mostaghimi, ''Deformation and solidification of molten particles on a substrate in thermal plasma spraying,'' Ref. 5, pp. 405–414.
[14]G. Trapaga and J. Szekely, ''Mathematical modeling of the isothermal impingement of liquid droplets in spraying processes,'' Metall. Trans. **22B**, 901 (1991).
[15]G. Trapaga, E. F. Matthys, J. J. Valencia, and J. Szekely, ''Fluid flow, heat transfer, and solidification of molten metal droplets impinging on substrates: Comparison of numerical and experimental results,'' Metall. Trans. **23B**, 701 (1992).
[16]J. Fukai, Z. Zhao, D. Poulikakos, C. M. Megaridis, and O. Miyatake, ''Modeling of the deformation of a liquid droplet impinging upon a flat surface,'' Phys. Fluids A **5**, 2588 (1993).
[17]L. M. Hocking and A. D. Rivers, ''The spreading of a drop by capillary action,'' J. Fluid Mech. **121**, 425 (1982).
[18]P. J. Haley and M. J. Miksis, ''The effect of the contact line on droplet spreading,'' J. Fluid Mech. **223**, 57 (1981).
[19]E. B. Dussan, V. E. Ramé, and S. Garoff, ''On identifying the appropriate boundary conditions at a moving contact line: An experimental investigation,'' J. Fluid Mech. **230**, 97 (1991).
[20]J. Fukai, Y. Shiiba, T. Yamamoto, O. Miyatake, D. Poulikakos, C. M. Megaridis, and Z. Zhao, ''Wetting effects on the spreading of a liquid droplet colliding with a flat surface: Experiment and modeling,'' Phys. Fluids **7**, 236 (1995).
[21]J. L. Bryan, *Fire Suppression and Detection Systems*, 3rd ed. (MacMillan, New York, 1993), pp. 331–334.
[22]B. D. Nichols, C. W. Hirt, and R. S. Hotchkiss, ''A solution algorithm for transient fluid flow with multiple free boundaries,'' Los Alamos Scientific Laboratory, LA-8355, UC-32, and UC-34 (1980).
[23]C. H. Chang, N. H. L. Wang, and E. I. Franses, ''Adsorption dynamics of single and binary surfactants at the air/water interface,'' Colloid. Surf. **62**, 321 (1992).
[24]C. H. Chang and E. I. Franses, ''Modified Langmuir–Hinshelwood kinetics for dynamic adsorption of surfactants at the air/water interface,'' Colloid. Surf. **69**, 189 (1992).
[25]P. D. Jontz and J. E. Myers, ''The effect of dynamic surface tension on nucleate boiling coefficients,'' AIChE J. **6**, 34 (1960).
[26]G. E. P. Elliot and A. C. Riddiford, ''Dynamic contact angles: I—The effect of impressed motion,'' J. Colloid Interface Sci. **23**, 389 (1967).
[27]R. L. Hoffman, ''A study of the advancing interface: I—Interface shape in liquid–gas systems,'' J. Colloid and Interface Science **50**, 228 (1975).
[28]V. P. Carey, *Liquid–Vapor Phase Change Phenomena* (Taylor & Francis, Bristol, PA, 1992), pp. 61–67.
[29]F. M. White, *Viscous Fluid Flow*, 2nd ed. (McGraw-Hill, New York, 1991), pp. 158–159.
[30]R. Bhola and S. Chandra, ''Freezing of droplets colliding with a cold surface,'' ASME HTD, 1995, Vol. 306, p. 181.